Revision 1

Iron-titanium oxyhydroxides as water carriers in the Earth's deep mantle

Yu Nishihara [1]* and Kyoko N. Matsukage [2]*

[1] Geodynamics Research Center, Ehime University, 2-5 Bunkyo-cho, Matsuyama, Ehime 790-8577, Japan

[2] Department of Earth and Planetary Sciences, Tokyo Institute of Technology, 2-12-1 Ookayama, Meguro-ku, Tokyo 152-8551 Japan

* These authors contributed equally to this work.

E-mail: yunishi@sci.ehime-u.ac.jp (Y.N.), matsukage.k.aa@m.titech.ac.jp (K.N.M.).

Submitted to *American Mineralogist*, 30 July 2015

revised 7 November 2015

ABSTRACT

We experimentally explored phase relations in the system FeOOH-TiO_2 at pressures of 16 GPa and temperatures of 1000–1600°C which corresponds to conditions of the Earth's mantle transition zone. Analyses of the recovered samples revealed that, in the studied conditions, there are two stable iron-titanium oxyhydroxide phases whose estimated composition is expressed by $(FeH)_{1-x}Ti_xO_2$. One is the Fe-rich solid solution ($x < 0.23$) with ε-FeOOH type crystal structure (orthorhombic, $P2_1nm$), and the other is the more Ti-rich solid solution ($x > 0.35$) with α-PbO_2 type structure (orthorhombic, *Pbcn*). The ε-FeOOH phase is stable up to ~1100ºC irrespective of chemical composition whereas the α-PbO_2 type phase is stable up to 1500ºC for a composition of $x = 0.5$ and at least to 1600ºC for $x = 0.75$, and thus the α-PbO_2 type phase is stable at average mantle temperature in the Earth's mantle transition zone. Iron-titanium-rich phases found previously in basalt + H_2O system are estimated to be the ε-FeOOH and α-PbO_2 type phases where the phase with iron-rich composition found at relatively low temperature (<1100ºC) is ε-FeOOH phase and the phase with titanium-rich composition is α-PbO_2 type phase. The α-PbO_2 type and ε-FeOOH phases may be stable in the sybducted basaltic crust at pressures in the mantle transition zone under water rich conditions even after being heated to the average mantle temperature.

Keywords: mantle transition zone, water, titanium, hydrous mineral, basaltic crust

INTRODUCTION

In the high-pressure and high-temperature environments of the Earth's mantle, water (or hydrogen) is considered to exist either as H_2O-rich fluids (or hydrous melts) or in minerals containing hydroxyl (OH) either as part of stoichiometric formulae or as a substantial defect in nominally anhydrous mineral formulae. These hydroxyl-containing

minerals may be transported by large-scale mantle convention to deeper parts of the mantle such as the mantle transition zone and the lower mantle, whereas the H_2O-rich fluids are thought to rise quickly to shallower parts (e.g. Ikemoto and Iwamori 2014). Due to the importance of water in the chemical and physical evolution of the mantle, the stability and water storage capacity of the H_2O bearing minerals in mantle rocks (peridotite) and subducted oceanic crusts (basalt) have been studied extensively (e.g. Kawamoto 2004; Okamoto and Maruyama 2004; Komabayashi and Omori 2006). Previous studies have revealed that the stability of hydrous minerals (e.g. antigorite, lawsonite, dense hydrous magnesium silicates) in these rock compositions is mostly restricted to temperatures lower than the average mantle temperature (e.g. Litasov and Ohtani 2005; Nishi et al. 2014). Although wadsleyite, which is the most abundant nominally anhydrous mineral in peridotitic mantle composition in the upper half of mantle transition zone, can incorporate up to 3.3 wt% water in its crystal structure at relatively low temperatures (<~1200ºC), its water content decreases to 0.4–0.5 wt% or less at average mantle temperature of ~1500ºC (Litasov et al. 2011). Lawsonite, which is the water-carrying phase in subducted basaltic crust, decomposes at depth exceeding 300 km (e.g. Schmidt and Poli 1998; Okamoto and Maruyama 2004), and thus, at the conditions in the mantle transition zone, the water storage capacity of the basaltic crust is thought to be restricted by water solubility of nominally anhydrous minerals such as clinopyroxene and garnet which is lower than ~0.1 wt% (e.g. Bromiley et al. 2004a; Mookhergee and Karato 2010). However, in most previous studies, the high-pressure and high-temperature experiments were carried out on simple systems where minor elements (such as Ti) were omitted.

In a recent experimental study on the connectivity of H_2O-rich fluids in a basalt + 3.5 wt% H_2O system with multiple component at pressure (P) of 10–12 GPa and

temperature (T) of 1000ºC (Matsukage et al. in prep.; Hashimoto and Matsukage 2013), we identified an iron-titanium-rich phase (FeTi-phase) whose weight total determined by chemical analyses using SEM-EDS (scanning electron microscope equipped with energy-dispersive spectrometer) turned out to be significantly lower than 100%, suggesting high water content of the phase (Fig. 1a, Table A1, see Appendix). While the presence of similar FeTi-phases has been reported in experiments on similar systems by previous studies, they were assumed to be anhydrous; Ono (1998) reported the presence of an unknown FeTi-phase at P = 9–15 GPa and T = 700–1200ºC in basalt + 6 wt% H_2O and sediment + 6 wt% H_2O systems and Okamoto and Maruyama (2004) reported the presence of a similar phase at P = 10–19 GPa and T = 700–1400ºC in a basalt + 2 wt% H_2O system. From the chemical data available, it would seem that these phases are previously unknown hydrous phases having chemical compositions in the Fe-Ti-O-H system, and that their stability field may possibly encompass a wide pressure and temperature range corresponding to the deeper part of the upper mantle and the mantle transition zone. However, their small grain sizes and relatively low abundance in the basalt (or sediment) + H_2O system has hindered efforts to determine their crystal structures or to confirm the presence of water.

Judging from relatively wide compositional range of the reported FeTi-phases [Ti/(Fe + Ti) = 0.1–1.0], the phase is considered to be solid-solution between Fe- and Ti-bearing end-members. Exchange reaction of $Fe^{3+} + H^+ \leftrightarrow Ti^{4+}$ seems to be possible because H^+ is small in size whereas any exchange reaction including Fe^{2+} is supposed to be more difficult. This exchange reaction has been proposed as the hydration reaction of rutile (Bromiley et al. 2004b; Bromiley and Hilairet 2005). Therefore we estimate that the FeTi-phases found in basalt (sediment) + H_2O systems have chemical composition in the FeOOH-TiO_2 system.

High-pressure and high-temperature phase relations in FeOOH and TiO_2 systems have been studied by some previous studies. In FeOOH system, it has been known that goethite (α-FeOOH) is stable at ambient condition and transforms to ε-FeOOH at above P = 5–6 GPa (Baneyeva and Bendeliani 1973; Gleason et al. 2008). Stability of these FeOOH polymorphs are limited to relatively low temperatures (e.g. up to T = 625°C at P = 7.7 GPa) and they decompose to hematite (Fe_2O_3) + water (H_2O) at higher temperatures. Previous studies on phase relation in TiO_2 system have established that, at T = 1000ºC, rutile-structured TiO_2 transforms to α-PbO_2 type structure phase at P = 8 GPa, which further transforms to baddeleyite-type structure phase (akaogiite) at P = 17 GPa (Akaogi et al. 1992; Tang and Endo 1993; Withers et al. 2003). On the other hand, almost nothing is known about phase stability for intermediate composition between FeOOH and TiO_2 at these conditions. A more systematic study in the FeOOH-TiO_2 system was needed for a deeper understanding of the FeTi-phase, which can be hydrous minerals in basalt and sediment compositions.

In this study, we experimentally explored phase relation in the system FeOOH-TiO_2 at P = 16 GPa and T = 1000–1600°C which corresponds to conditions of the Earth's mantle transition zone. Based on the experimental results, we discuss potential importance of the iron-titanium oxyhydroxides in the subducted basaltic crust in the transition zone.

EXPERIMENTAL METHODS

High-pressure and high-temperature experiments

We performed synthesis experiments on the iron-titanium oxyhydroxides with seven different compositions in the FeOOH-TiO_2 system having molar ratios of x = Ti/(Fe + Ti) = 0, 0.125, 0.25, 0.375, 0.5, 0.75 and 1. Starting materials were prepared by mixing

reagent grade α-FeOOH (goethite) and TiO_2 (anatase) powders. The powder mixture were ground with an agate mortar and pestle. Au tubes (OD: 1.5 mm, ID: 1.3 mm, where OD and ID are outer and inner diameters, respectively) or $Au_{75}Pd_{25}$ tubes (OD: 1.3 mm, ID: 1.1 mm) were used as sample capsules, and the ends were welded to provide sealing for the hydrous fluid. The oxygen fugacity (f_{O2}) in the sample is expected to be very high because (1) iron in the starting material is supplied by $Fe^{3+}OOH$ and (2) possible leakage of hydrogen from capsule through diffusion in AuPd (or Au) makes sample environment more oxidative.

High-pressure and high-temperature experiments were carried out using an Kawai-type multi-anvil apparatus (ORANGE-1000) installed at Ehime University at P = 16 GPa and T = 1000–1600ºC (Table 1), which correspond to the conditions of the upper part of the mantle transition zone. An (Mg,Co)O octahedral pressure medium with edge length of 14 mm and eight tungsten carbide anvils with truncation edge length of 8 mm were employed for the experiments. The samples were heated using tubular $LaCrO_3$ heater (OD: 5.5 mm, ID: 3.5 mm, 8.0 mm long), and temperature was monitored using W3Re-W25Re thermocouple. Pressure was calibrated with the phase transition of Bi (I-II, III-V) and ZnTe (Kusaba et al. 1993) at room-temperature and SiO_2 (coesite-stishovite, Zhang et al. 1996) and Mg_2SiO_4 (olivine-wadsleyite, Morishima et al. 1994) at high-temperature (1300–1600ºC). Precision of the pressure estimates is believed to be within 5%. Temperature variation within each sample capsule is estimated to be ~100ºC based on the calibration using pyroxene thermometry (Matsukage et al., in prep.). Two or four capsules were employed simultaneously in the experiments of the $FeOOH$-TiO_2 system (Supplementary materials, Fig. S1). The samples packed in Au or AuPd capsules were compressed to target pressure. Then the capsules were heated to the target temperature, kept there for 15–600 min, and

147 recovered to ambient condition.

148

149 **Analyses on recovered samples**

150 The recovered samples were polished to expose their central part, and analyzed by
151 X-ray diffraction (XRD) for phase identification, by Fourier-transform infrared
152 spectroscopy (FT-IR) to examine presence of hydroxyl, and by SEM-EDS for
153 microstructure observation and quantitative chemical analyses. XRD analyses were
154 performed using RIGAKU RINT RAPIDII equipped with rotative anode (Cu $K\alpha$
155 radiation), two-dimensional imaging plate detector and ϕ100 μm collimator. Typical
156 exposure time in the XRD analyses was 300 s.

157 FT-IR analyses were conducted using Perkin Elmer Spectrum One in reflection
158 mode. Measurements were carried out using mid-IR light, a KBr beam splitter and an
159 MCT detector. Non-polarized IR beam with dimension of 100 × 100 μm^2 was used. A
160 gold mirror was used as a standard reference for the reflection measurements. The IR
161 spectra were obtained from 200 integrated scans with 4 cm^{-1} resolution. The
162 Kramers-Krönig conversion was applied to the reflection FT-IR spectra to obtain
163 absorption coefficient spectra. In general, FT-IR analyses on minerals containing
164 hydroxyl are carried out with transmission mode using a doubly polished thin section or
165 a pellet made of mixture of sample powder and KBr. However, after some trial analyses
166 by transmission mode, we recognized that FT-IR analyses on present samples with
167 transmission mode are not impossible but difficult because most samples are highly
168 opaque and fragile. Note that absorption coefficient derived by the Kramers-Krönig
169 conversion of the reflection spectra are semi-quantitative unlike that determined directly
170 by transmission mode. Comparison of FT-IR spectra taken by reflection and
171 transmission modes are presented in Supplementary materials (Supplementary materials,

Fig. S2).

SEM-EDS analyses were carried out using JSM-6480 equipped with LaB_6 filament installed at Kobe University. Chemical analyses were performed with 15 kV accelerating voltage, 0.4 nA beam current, integration counting time of 100 s, and working distance of 10 mm with ZAF correction. Standards used in this study were hematite for Fe and rutile for Ti. The beam current was adjusted just before each measurement in order to maximize accuracy in the chemical analysis. Water contents in individual phases were estimated from total deficits in SEM-EDS analyses assuming all iron is ferric (Fe^{3+}).

RESULTS

Two different hydrous phases were found to be stable in the studied conditions. One is the Fe-rich solid solution with ε-FeOOH type crystal structure, and the other is the Ti-rich solid solution with α-PbO_2 type structure.

Phase relations

Fig. 2 shows the phase diagram in the FeOOH-TiO_2 system at P = 16 GPa determined in this study. At temperatures below T = 1100ºC, the ε-FeOOH phase is stable for relatively Fe-rich compositions (x = Ti/(Ti + Fe) < 0.23), and the α-PbO_2 type phase is stable over a wide compositional range of x > 0.35, and the two phases coexist at compositions between the single-phase stability fields (Fig. 1b). At 1100ºC, the ε-FeOOH phase decomposes to hematite + H_2O fluid; the decomposition temperature has very small compositional dependence. There was no notable change in the phase relation at 1200–1500ºC where Ti-bearing hematite (Fe_2O_3) + H_2O and α-PbO_2 type phase exist stably at x < ~0.1 and x > 0.5, respectively, with the field of α-PbO_2 type

197 phase + hematite + H_2O coexisting between them (Fig. 1c). At 1600ºC, an oxide-bearing
198 melt with chemical composition of $x = 0.2–0.3$ appears and the stability field of α-PbO_2
199 type phase starts to recede to the Ti-rich side (Fig. 1d), although the α-PbO_2 type phase
200 remains stable at $x > 0.6$.

201 Chemical composition determined by SEM-EDS analyses are shown in Table 2 and
202 Fig. 3. The measured chemical composition of individual phases is consistent with the
203 phase diagram constructed based on phase assemblage (Fig. 2) except for that of
204 α-PbO_2 type phase. The composition of the α-PbO_2 type phase coexisting with hematite
205 + H_2O at temperatures of 1200–1500ºC varied between $x = 0.23$ and 0.53 depending on
206 the bulk composition although the α-PbO_2 type phase is expected to have unique
207 composition when the system is expressed by Fe_2O_3-TiO_2-H_2O three component system.
208 This discrepancy is discussed in a later section.
209

210 **ε-FeOOH phase**

211 The X-ray diffraction peaks for the ε-FeOOH phase solid solution are indexed based
212 on the ε-FeOOH structure (orthorhombic, $P2_1nm$) (Fig. 4a). The calculated lattice
213 parameters for the ε-FeOOH end-member (Supplementary materials, Table S1) are
214 consistent with previously reported values (Suzuki 2010). The lattice parameters appear
215 to be almost independent of chemical composition (Table S1), although it must be noted
216 that the compositional range of this phase is rather limited ($1 \leq x \leq 0.23$).

217 The presence of strong absorption peak in FT-IR spectra near 2860 cm^{-1} and smaller
218 peaks at ~2230 and ~1870–1890 cm^{-1} is indicative of high water (hydroxyl)
219 concentration in this phase (Fig. 5). The wavenumber of the FT-IR peaks is lower than
220 general values for O-H stretching frequencies in hydroxyl-containing minerals
221 (3000–3800 cm^{-1}). However, the our results are reasonable because known

222 oxyhydroxides with same crystal structure as ε-FeOOH (δ-AlOOH, γ-MnOOH and
223 InOOH) consistently show very low O-H stretching frequencies (2100–2800 cm^{-1}) due
224 to short distance of O-H…O hydrogen bond (e.g. Kohler et al. 1997; Xue and Kanzaki
225 2007; Tsuchiya et al. 2008). H_2O contents in this phase have been determined by weight
226 deficiency in SEM-EDS analyses to be ~10 wt% and are found to be consistent with
227 stoichiometirc values for solid solutions in the FeOOH-TiO_2 system (Table 2 and Fig. 6).
228 Previously reported data on low temperature phase relations (<500ºC) in a pure FeOOH
229 system (Baneyeva and Bendeliani 1973; Gleason et al. 2008) are generally consistent
230 with this study, while the dissolution of TiO_2 component into ε-FeOOH phase reported
231 here has not been previously known.
232
233 **α-PbO_2 type phase**
234 The XRD patterns of the α-PbO_2 type phase solid solution are indexed as an α-PbO_2
235 structure (orthorhombic, *Pbcn*) (Fig. 4b). The calculated lattice parameters exhibit
236 strong compositional dependence, where *b* and *c* decrease and *a* increases with
237 increasing TiO_2 content (Fig. 7 and Table S1). The intensity of the broad FT-IR
238 absorption peak at ~2860–2880 cm^{-1} and smaller peaks at ~2300–2315 and 1800–1885
239 cm^{-1} (corresponding to O-H stretching vibration) decreases with increasing TiO_2
240 content, and the peak vanishes in pure TiO_2 (Fig. 5), which is to be expected from the
241 fact that hydroxyl content is proportional to iron content in the FeOOH-TiO_2 binary
242 system. The relatively low O-H frequencies (<~2900 cm^{-1}) suggests short distance of
243 O-H…O hydrogen bond (<~2.7 Å) in this phase (Nakamoto et al. 1955). The SEM-EDS
244 analyses clearly show that all α-PbO_2 type phases have nearly stoichiometric H_2O
245 contents except for one sample at 1600ºC (starting material composition: x = 0.375)
246 (Table 2 and Fig. 6).

The α-PbO_2 type phase is stable on the TiO_2-rich side at P = 16 GPa, which is consistent with previous studies on phase relation in TiO_2 system (Akaogi et al. 1992; Tang and Endo 1993; Withers et al. 2003). Based on annealing experiments at P = 6 and 7 GPa and T = 1100ºC, Bromiley et al. (2004b) reported low solubility of hydrogen (0 wt ppm H_2O) in α-PbO_2 type TiO_2 under Fe_2O_3-saturated condition, in contrast, our results show that substantial amount of FeOOH component dissolves into α-PbO_2 type TiO_2 at P = 16 GPa. This suggests a strong pressure dependence of FeOOH solubility in the α-PbO_2 type TiO_2. Our results show that, at P = 16 GPa, the α-PbO_2 type phase is stable up to T = 1500ºC for a composition of x = 0.5 and at least to T = 1600ºC for x = 0.75, and thus this phase is stable at average mantle temperature in the Earth's mantle transition zone. The temperatures reported here are the highest known temperatures for the stability of hydrous minerals, except for the hydrous δ-phase (AlOOH-$MgSiO_2(OH)_2$) which has been found to be stable at lower mantle conditions (Ohira et al. 2014; Walter et al. 2015).

Detailed SEM-EDS analyses have revealed (1) the presence of exsolution lamellae in the α-phase and (2) the coexistence of two α-PbO_2 type phase "-like" phases with similar but distinct chemical compositions in some samples at relatively high temperatures (1400–1600ºC, Table 2 and Fig. 3). No indications of additional structurally-different phase was confirmed in either XRD or FT-IR data for these samples. The exsolution lamellae exhibit fine microstructure (<2 μm) and are considered to be formed during quenching from a homogeneous single phase that is stable at high temperature. The coexistence of two α-PbO_2 type phases with relatively close chemical compositions is observed when H_2O fluid or melt is present in the system, and the two α-PbO_2 type phases are found separately at high- and low-temperature parts of the capsule (Fig. 1d). These observations suggest that the

presence of the two α-PbO_2 type phases is attributable to the presence of a temperature gradient in the capsule and also to a strong temperature dependence of the α-PbO_2 type phase composition coexisting with hematite and fluid (or melt) at around T ~ 1500–1600ºC. An alternative interpretation for the above observation is the possible stability of an unknown phase whose crystal structure is related to the α-PbO_2 type and that transforms to the α-PbO_2 type phase during temperature and/or pressure release stage.

Although the formation process of the lamellae and the two compositionally different phases remains unclear, we conclude that the hydrous phase having $(FeH)_{1-x}Ti_xO_2$ stoichiometry is stable over a wide range of temperature conditions and compositions and is capable of retaining up to 8.0 wt% water at maximum.

Hematite

In FT-IR spectra of hematite, no detectable peak was observed at 1500–3800 cm^{-1} indicating absence of hydroxyl (Fig. 5). TiO_2 content in hematite is relatively limited and is 12 wt% at the maximum (Table 2). Weight total of hematite in SEM-EDS analyses was systematically high and was 100.0–103.6%. On the other hand, single crystal pure hematite ($Fe^{3+}{}_2O_3$) of analytical standard was analyzed repeatedly among measurements on present samples, and it always showed weight total close to 100% (99.5–100.5%). The systematically high weight total of hematite in present samples may be suggesting presence of Fe^{2+} in the experimental hmatite.

DISCUSSION

Interpretation of phase relations

In the Fe_2O_3-TiO_2-H_2O three component system, the α-phase with $(FeH)_{1-x}Ti_xO_2$

297 stoichiometry coexisting with hematite and H_2O fluid should, in principle, have unique
298 composition regardless of bulk composition at a given pressure and temperature
299 condition. However, the measured composition of the α-PbO_2 type phase at T =
300 1200–1500ºC varied between x = 0.23 and 0.53 depending on the bulk composition
301 (Table 2 and Fig. 3). This is presumably due to the deviation of the system from a pure
302 three component system resulting from the presence of O_2 component in fluid and/or
303 Fe^{2+}-bearing component(s) in the α-PbO_2 type phase and/or hematite (such as $Fe^{2+}TiO_3$).
304 Another possible explanation for the above phenomenon is the deviation of α-PbO_2 type
305 phase composition from the $(FeH)_{1-x}Ti_xO_2$ stoichiometry. In this study, we discuss the
306 stability field of the α-PbO_2 type phase based on the phase diagram constructed from
307 phase assemblage (Fig. 2) for the sake of simplicity. Further exploration on crystal
308 chemistry of the α-PbO_2 type phase, including the valence state of iron, remains to be
309 investigated.

310 In this study, f_{O2} in the samples was not controlled by external buffer. The f_{O2} in
311 present experiments is considered to be high because all iron is Fe^{3+} in the starting
312 materials and some amount of hydrogen may be leaked from sample by diffusion in
313 $Au_{75}Pd_{25}$ (and Au) capsule. Under lower f_{O2} which corresponds to the Earth's mantle
314 conditions, phase relation in the FeOOH-TiO_2 system may be significantly different
315 from that determined in this study. However, we observed presence of the FeTi-mineral
316 in basalt + H_2O system under controlled f_{O2} of Ni-NiO buffer that is generally regarded
317 to be close to mantle f_{O2} (Fig. 1a, see Appendix, Matsukage et al., in prep.; Hashimoto
318 and Matsukage, 2013). Therefore the iron-titanium oxyhydroxide(s) is considered to be
319 stable under relatively wide range of f_{O2}.
320

321 **Implications for water transport in the deep Earth's mantle**

Judging from the phase relation in the FeOOH-TiO_2 system at P = 16 GPa (Fig. 2), the FeTi-phases found in a basalt + H_2O system (Fig. 1a, Ono, 1998; Okamoto and Maruyama, 2004) are deduced to be the ε-FeOOH and α-PbO_2 type phases where the phase with iron-rich composition found at relatively low temperature (<1100ºC) is the ε-FeOOH phase and the phase with titanium-rich composition is the α-PbO_2 type phase. Fig. 8 compares stability fields of the FeTi-phases and other hydrous phases in basalt + H_2O and peridotite + H_2O systems and temperature profiles in the mantle (mantle adiabat and slab surface temperature). The information available from previous studies and from our study implies that both ε-FeOOH and α-PbO_2 type phases are stable in the subducted basaltic crust at pressures in the mantle transition zone (410–660 km depth) under water saturated conditions even after being heated to the average temperature. Although the modal abundances of ε-FeOOH and α-PbO_2 type phases in basalt system are limited due to the relatively low TiO_2 contents in basalts (1–2 wt% TiO_2 for mid-oceanic-ridge basalt, Gale et al. 2013; White and Klein 2014), the presence of these phases with high water content (up to 10 wt% H_2O) will allow subducted basaltic crusts to retain certain amounts of water in the transition zone.

The α-PbO_2 type SiO_2 is one of the major constituent minerals (~20 wt%) in basaltic systems at pressures above 110 GPa (e.g. Hirose et al. 2005). Bromiley et al. (2004b) discussed that solubility of H and Al in the α-PbO_2 type SiO_2 would be very low based on their experimental results on the very low solubility of H and Fe^{3+} in the α-PbO_2 type TiO_2 at 6 and 7 GPa. In contrast, we discovered that, at 16 GPa, the α-PbO_2 structure phase in FeOOH-TiO_2 system is stable over a wide compositional range. This suggests that significant dissolution of FeOOH (and/or AlOOH) component into a SiO_2 phase with α-PbO_2 structure may occur as well as TiO_2. Therefore the water storage capacity in the subducted basaltic crust can be expected to be quite high, say 2

wt% H_2O, at the bottom of lower mantle.

ACKNOWLEDGEMENTS

We thank Y. Seto for his technical assistance in analyses using scanning electron microscope, and M. Hashimoto, K. Fuke, T. Shinmei and T. Inoue for their assistance in sample preparation and high-pressure and high-temperature experiments. This work was supported by Grant-in-Aid for Scientific Research (B) (22340161) and for Scientific Research on Innovative Areas (21109004), and Women's Future Development Center in Ehime University. Constructive comments by G. Bromiley and T. Kawamoto are appreciated.

Author Contributions

Y.N. performed the high-pressure experiments, X-ray diffraction and FT-IR measurements. K.N.M. discovered the iron-titanium oxyhydroxides in basalt + H_2O system, and performed SEM-EDS analysis. Both authors designed the research methodology, wrote the paper, and approved the final manuscript.

REFERENCES CITED

Akaogi, M., Kusaba, K., Suzuki, T., Yagi, T., Matsui, M., Kikegawa, T., Yusa, H., and Ito, E. (1992) High-pressure high temperature stability of αPbO_2-type and $MgSiO_3$ majorite: calorimetric and *in situ* X-ray diffraction studies. In Syono, Y., Manghnani, M.H. (Eds.), High Pressure Research: Application to Earth and Planetary Sciences. In: Geophys. Monogr., Vol. 67. American Geophysical Union, Washington D.C., pp. 447-455.

Baneyeva, M.I. and Bendeliani, N.A. (1973) The Fe_2O_3-H_2O system at high pressures

and extemperatures. Geochemistry International, 10, 840-842.

Brown, J.M. and Shankland, T.J. (1981) Thermodynamic parameters in the Earth as determined from seismic profiles. Geophysical Journal of the Royal Astronomical Society, 66, 579-596.

Bromiley, G.D. and Hilairet, N. (2005) Hydrogen and minor element incorporation in synthetic rutile. Mineralogical Magazine, 69, 345-358.

Bromiley, G.D., Keppler, H., McCammon, C., Bromiley, F.A., and Jacobsen, S.D. (2004a) Hydrogen solubility and speciation in natural gem-quality chromian diopside. American Mineralogist, 89. 941-949.

Bromiley, G., Hilaret, N., and McCammon, C. (2004b) Solubility of hydrogen and ferric iron in rutile and TiO_2 (II): implications for phase assemblages during ultrahigh-pressure metamorphism and for the stability of silica polymorphs in the lower mantle. Geophysical Research Letters, 31, doi:10.1029/2004GL019430.

Gale, A., Dalton, C.A., Langmuir, C.H., Su, Y., and Schilling, J.-G. (2013) The mean composition of ocean ridge basalts. Geochemistry Geophysics Geosystems, 14, doi:10.1029/2012GC004334.

Gleason, A.E., Jeanloz, R., and Kunz, M. (2008) Pressure-temperature stability studies of FeOOH using X-ray diffraction. American Mineralogist, 93, 1882-1885.

Hashimoto, M. and Matsukage, K.N. (2013) Dihedral angle of garnet-H_2O fluid in eclogite: implication for low S-wave velocity regions at lowermost upper mantle. Japan Geoscience Union Meeting 2013 abstracts, SCG63-P08.

Hirose, K., Takafuji, N., Sata, N., and Ohishi, Y. (2005) Phase transition and density of subducted MORB crust in the lower mantle. Earth and Planetary Science Letters, 237, 239-251.

Ikemoto, A. and Iwamori, H. (2014) Numerical modeling of trace element

transportation in subduction zones: implications for geofluid processes. Earth Planets Space, 66:26.

Katsura, T., Yoneda, A., Yamazaki, D., Yoshino, T., and Ito, E. (2010) Adiabatic temperature profile in the mantle. Physics of the Earth and Planetary Interiors, 183, 212-218.

Kawamoto, T. (2004) Hydrous phase stability and partial melt chemistry in H_2O-saturated KLB-1 peridotite up to the uppermost lower mantle conditions. Physics of the Earth and Planetary Interiors, 143-144, 387-395.

Kohler, T., Armbruster, T., and Libowitzky, E. (1997) Hydrogen bonding and Jahn-Teller distortion in groutite, α-MnOOH and manganite, γ-MnOOH, and their relations to the manganese dioxides ramsdellite and pyrolusite. Journal of Solid State Chemistry, 133, 486-500.

Komabayashi, T. and Omori, S. (2006) Internally consistent thermodynamic data set for dense hydrous magnesium silicates up to 35 GPa, 1600°C: implications for water circulation in the Earth's deep mantle. Physics of the Earth and Planetary Interiors, 156, 89-107.

Kusaba, K., Galoisy, L., Wang, Y., Vaughan, M.T., and Weidner, D.J. (1993) Determination of phase transition pressures of ZnTe under quasihydrostatic conditions. Pure and Applied Geophysics, 141, 643-651.

Litasov, K.D. and Ohtani, E. (2005) Phase relations in hydrous MORB at 18-28 GPa: implications for heterogeneity of the lower mantle. Physics of the Earth and Planetary Interiors, 150, 239-263.

Litasov., K.D., Shatskiy, A., Ohtani, E., and Katsura, T. (2011) Systematic study of hydrogen incorporation into Fe-free wadsleyite. Physics and Chemistry of Minerals, 38, 75-84.

Morishima, H., Kato, T., Suto, M., Ohtani, E., Urakawa, S., Utsumi, W., Shimomura, O., and Kikegawa, T. (1994) The phase boundary between α- and β-Mg_2SiO_4 determined by in situ X-ray observation. Science, 265, 1202-1203.

Mookhergee, M. and Karato, S. (2010) Solubiliy of water in pyrope-rich garnet at high pressures and temperatures. Geophysical Research Letters, 37, doi:10.1029/2009GL041289.

Nakamoto, K., Margoshes, M., and Rundle, R.E. (1955) Stretching frequencies as a function of distances in hydrogen bonds. Journal of American Chemical Society, 77, 6480-6486.

Nishi, M., Irifune, T., Tsuchiya, J., Tange, Y., Nishihara, Y., Fujino, K., and Higo, Y. (2014) Stability of hydrous silicate at high pressures and water transport to the deep lower mantle. Nature Geoscience, 7, 224-227.

Nishio-Hamane, D., Shimzu, A., Nakahira, R., Niwa, K., Sano-Furukawa, S., Okada, T., Yagi, T., and Kikegwa, T. (2010) The stability and equation of state for the cotunnite phase of TiO_2 up to 70 GPa. Physics and Chemistry of Minerals, 37, 129-136.

Ohira, I., Ohtani, E., Sakai, T., Miyahara, M., Hirao, N., Ohishi, Y., and Nishijima, M. (2014) Stability of a hydrous δ-phase, AlOOH-$MgSiO_2(OH)_2$, and a mechanism for water transport into the base of lower mantle. Earth and Planetary Science Letters, 401, 12-17.

Okamoto, K. and Maruyama, S. (2004) The eclogite-garnetite transformation in the MORB + H_2O system. Physics of the Earth and Planetary Interiors, 146, 283-296.

Ono, S. (1998) Stability limits of hydrous minerals in sediment and mid-oceanic ridge basalt compositions: implications for water transport in subduction zones. Journal of Geophysical Research, 103, 18253-18267.

Schmidt, M.W. and Poli, S. (1998) Experimentally based water budgets for dehydrating

slabs and consequences for arc magma generation. Earth and Planetary Science Letters, 163, 361-379.

Simons, P.Y. and Dachille, F. (1967) The structure of TiO_2 II, a high-pressure phase of TiO_2. Acta Crystallographica, 23, 334-336.

Suzuki, A. (2010) High-pressure X-ray diffraction study of ε-FeOOH. Physics and Chemistry of Minerals, 37, 153-157.

Syracuse, E.M., van Keken, P.E., and Abers, G.A. (2010) The global range of subduction zone thermal models. Physics of the Earth and Planetary Interiors, 183, 73-90.

Tang, J. and Endo, S. (1993) *P-T* boundary of α-PbO_2 type and baddeleyite type high-pressure phases of titanium dioxide. Journal of American Ceramic Society, 76, 796-798.

Tsuchiya, J., Tsuchiya, T., and Wentzcovitch, R.M. (2008) Vibrational properties of δ-AlOOH under pressure. American Mineralogist, 93, 477-482.

Walter, M., Thomson, A.R., Wang, W., Lord, O.T., Ross, J., McMahon, S.C., Baron, M.A., Melekhova, E., Kleppe, A.K., and Kohn, S.C. (2015) The stability of hydrous silicates in Earth's lower mantle: experimental constraints from the system $MgO-SiO_2-H_2O$ and $MgO-Al_2O_3-SiO_2-H_2O$. Chemical Geology, in press.

White, W.M. and Klein, E.M. (2014) Composition of the oceanic crust. In: Rudnick, R.L. (Ed.), Treatise on Geochemistry 2nd Edition Vol. 4 The Crust, Elsevier, Amsterdam, pp. 457-496.

Withers, A.C., Essene, E.J., and Zhang, Y. (2003) Rutile/TiO_2II phase equilibria. Contributions to Mineralogy and Petrology, 145, 199-204.

Xue, X. and Kanzaki, M. (2007) High-pressure δ-$Al(OH)_3$ and δ-AlOOH phases and isostructural hydroxides/oxyhydroxides: new structural insights from

high-resolution ^{1}H and ^{27}Al NMR. The Journal of Physics and Chemistry B, 111, 13156-13166.

Zhang, J., Li, B., Utsumi, W., and Liebermann, R.C. (1996) In situ X-ray observations of the coesite-stishovite transition: reversed phase boundary and kinetics. Physics and Chemistry of Minerals, 23, 1-10.

FIGURE CAPTIONS

Figure 1. Back-scattered electron images of samples. (a) OD1168 (basalt + 3.5 wt% H_2O) at 12 GPa, 1000ºC; (b) OD1292-3 (starting material composition: x = Ti/(Fe + Ti) = 0.25 in FeOOH-TiO_2 system) at 16 GPa, 1000ºC; (c) OD1334-2 (x = 0.5) at 16 GPa, 1400ºC; (d) OD1338-2 (x = 0.5), at 16 GPa, 1600ºC. Cpx: clinopyroxene; Grt: garnet; FeTi: FeTi-phase; α: α-PbO_2 type phase; ε: ε-FeOOH phase; Hem: hematite.

Figure 2. Phase diagram of FeOOH-TiO_2 pseudo-binary system at pressure of 16 GPa. Symbol colors represent stable phases. Red: α-PbO_2 type phase solid solution; light blue: ε-FeOOH solid solution; green: hematite + H_2O; and purple: melt or hematite + melt. Black dots show chemical compositions of coexisting phases under subsolidus condition. The α-PbO_2 type phase has a wide stability field on the TiO_2-rich side [Ti/(Fe + Ti) = 0.35–1] up to very high temperature (1600ºC), whereas the stability of ε-FeOOH solid solution is limited to the FeOOH-rich side [Ti/(Fe + Ti) = 0–0.2] and below 1100ºC.

Figure 3. Compositions [Ti/(Fe + Ti) in molar ratio] of phases in recovered samples. Same colors as Fig. 2 are used to represent phases (green: hematite; purple melt). Large and small symbols represent presence and absence of coexisting phase except for H_2O, respectively. Gray lines represent phase boundaries determined from phase assemblage (same as black lines in Fig. 2). Asterisks indicate the presence of exsolution lamellae. Red lines connecting symbols indicate pairs of coexisting α-PbO_2-like phases having different compositions, and H and L denote the composition of the pair having higher and lower TiO_2 content, respectively. Formation process of the lamellae and the coexistence of two compositionally different α-PbO_2-like phases is not clear (see text).

503

504 Figure 4. Representative X-ray diffraction patterns of (a) ε-FeOOH (OD1288-1) phase
505 and (b) α-PbO_2 type phase (top: OD1292-4, bottom: OD1292-5) in the FeOOH-TiO_2
506 system. Value *x* is defined as *x* = Ti/(Fe + Ti). Numbers attached to peaks are Miller
507 indices. Asterisks correspond to peaks for capsule materials (Au or AuPd alloy).

508

509 Figure 5. FT-IR spectra of ε-FeOOH (*x* = 0 and 0.143 are from OD1347-6 and
510 OD1347-1, respectively) and α-PbO_2 type (*x* = 0.384, 0.521, 0.757 and 1 are from
511 OD1347-4, OD1334-2, OD1336-5 and OD1336-7, respectively) phases in the system
512 FeOOH-TiO_2 and hematite (OD1347-6) after Kramers-Krönig conversion of spectra
513 taken with the reflection method. The presence of strong absorption peak at 1800–2900
514 cm^{-1} (except for α-PbO_2 type TiO_2 and hematite) demonstrates high concentration of
515 water (hydroxyl) in these phases. Asterisks are noise from H_2O and CO_2 in air.

516

517 Figure 6. H_2O content of α-PbO_2 type phase (solid symbols and crosses) and ε-FeOOH
518 phase (open symbols). The line represents the stoichiometric H_2O content calculated for
519 the solid solution in the FeOOH-TiO_2 binary system. Asterisks attached to symbols for
520 α-PbO_2 type phase indicate the presence of exsolution lamellae. The measured H_2O
521 content for the two phases are consistent with the stoichiometric composition, except for
522 highest temperature samples (1600ºC).

523

524 Figure 7. Lattice parameters of α-PbO_2 type phase solid solution in the system
525 FeOOH-TiO_2 as a function of chemical composition. Open squares, solid triangles and
526 solid circles represent data of samples synthesized at 1000, 1400 and 1500ºC,
527 respectively. Crosses represent data for α-PbO_2 type TiO_2 reported in previous studies

(Simons and Dachille, 1967; Nishio-Hamane et al., 2010). Strong compositional dependence of lattice parameters are clearly evident, in which *b* and *c* decrease and *a* increases with increasing TiO_2 content.

Figure 8. Pressure and temperature diagram showing stability of hydrous phases. Solid and open squares represent the stability of α-PbO_2 type and ε-FeOOH phases in the FeOOH-TiO_2 system, respectively (this study). Solid circle, open circles and open diamonds represent the stability of iron-titanium rich phases in basalt + H_2O system reported in this study (Matsukage et al., in prep.), Okamoto and Maruyama (2004) and Ono (1998), respectively. Red and green lines represent the stability of hydrous phases in basalt + H_2O (Okamoto and Maruyama, 2004) and peridotite + H_2O (Kawamoto, 2004) systems, respectively. Bold black lines and blue lines with hatch correspond to be the mantle adiabat (B & S, Brown and Shankland, 1981; K et al., Katsura et al., 2010) and global range of slab surface temperature (Syracuse et al., 2010), respectively. Abbreviations are, Law: lawsonite; Ser: serpentine; CH: clinohumite; Ph A: phase A; Ph E: phase E; Ph D: phase D; Shy B: superhydrous phase B; Wd: wadsleyite; and Rw: ringwoodite.

APPENDIX

Iron-titanium mineral in basalt + H_2O composition

In our recent experimental study on the connectivity of H_2O-rich fluids, we identified iron-titanium-rich phases in a basalt + 3.5 wt% H_2O system at P = 10 and 12 GPa and T = 1000ºC (Matsukage et al. in prep.; Hashimoto and Matsukage 2013). The high-pressure and high-temperature experiments were carried out based on the similar method as that used in this study. The starting material of the basalt + 3.5 wt% H_2O were prepared by mixing JB-2 basalt powder (geochemical reference material, Geological Survey of Japan) and a reagent grade of $Mg(OH)_2$. The basalt + 3.5 wt% H_2O was packed in an Au capsule (OD: 1.5 mm, ID: 1.3 mm), and the Au capsule was further packed in a Pt capsule (OD: 1.8 mm, ID: 1.6 mm) together with Ni + NiO + $Ni(OH)_2$ mixture (with weight ratio of 10 : 3 : 3) to control oxygen fugacity (f_{O2}) during experiments. Both the Au and Pt capsules were sealed by welding. Experimental duration was 24 h.

The SEM-EDS analyses revealed that both samples at 10 and 12 GPa consist of garnet, clinopyroxene, coesite or stishovite, FeTi-phase(s) and fluid (Fig. 1a). Presence of both Ni and NiO in the recovered f_{O2} buffer material were observed suggesting that sample f_{O2} was controlled by the Ni-NiO reaction throughout experiments. Weight total of the FeTi-rich minerals determined by chemical analyses using SEM-EDS turned out to be significantly lower than 100%, suggesting high water content of the phase (Table A1). Two chemically distinct FeTi-phases were observed in the sample at 12 GPa suggesting coexistence of ε-FeOOH and α-PbO_2 type phases (Table A1).

Table 1. Experimental conditions and results of experiments in the FeOOH-TiO_2 system

Run#	Temperature (^oC)	Run time (min)	Strating material [a] Ti/(Fe + Ti)	Phase [b]
OD1288 -1	1000	600	0.125 [#]	ε
-2			0.5 [#]	α
OD1292 -3	1000	570	0.25	$\varepsilon + \alpha$
-4			0.375	α
-5			0.75	α
-6			0	ε + Hem(tr)
OD1347 -1	1100	300	0.125	ε + Hem*(tr) +H_2O
-3			0.25	$\varepsilon + \alpha$ + Hem* + H_2O
-4			0.375	α
-6			0	ε + Hem + H_2O
OD1291 -1	1200	300	0.125	α + Hem + H_2O
-2			0.5	α + Hem(tr)
-3			0.25	α + Hem + H_2O
-4			0.375	α + Hem + H_2O
OD1298 -2	1300	90	0.5	α + Hem(tr)
-3			0.25	α + Hem + H_2O
-5			0.75	α
OD1334 -1	1400	45	0.125	α_H* + α_L + Hem + H_2O
-2			0.5	α + Hem(tr)
-3			0.25	α + Hem + H_2O
-5			0.75	α
OD1336 -1	1500	30	0.125	α* + Hem + H_2O
-2			0.5	$\alpha_H + \alpha_L$ +Hem(tr)
-5			0.75	α

	-7			1	α
OD1338	-1	1600	15	0.125	Hem + Melt
	-4			0.375	α_H* + α_L* + Melt
	-2			0.5	α_H + α_L + Melt
	-5			0.75	α

All runs were made at pressure of 16.0 GPa.

a Runs using Au capsules indicated with superscript "#"; $Au_{75}Pd_{25}$ capsules were used in all other experiments.

b Abbreviations are α: α-PbO_2 type phase; ε: ε-FeOOH phase; Hem: Hematite; H_2O: H_2O fluid; Melt: oxide-bearing melt; tr: trace. α_H and α_L represent pairs of coexisting α-PbO_2-like phases with higher and lower Ti contents, respectively. The superscript "*" denotes the presence of exsolution lamellae.

Table 2. Compostion of individual phases in run products

Run#	Stariting material Ti/(Fe + Ti)	Phase	*n* [a]	Weight % TiO_2	Fe_2O_3	H_2O [b]	Total	Atomic ratio O	Ti	Fe	H [b]	Fe + Ti	Ti/(Fe + Ti)
T = 1000ºC													
OD1292-6	0	ε	6	0.2 (0.1)	89.1 (2.1)	10.7 (2.1)	100.0	2	0.00 (0.00)	0.98 (0.02)	1.05 (0.21)	0.98	0.002
		Hem	1	0.1	102.9		103.0	3	0.00	2.00	0.00	2.00	0.001
OD1288-1	0.125	ε	9	12.2 (0.5)	79.2 (1.0)	8.6 (1.3)	100.0	2	0.13 (0.01)	0.87 (0.01)	0.84 (0.13)	1.01	0.133
OD1292-3	0.25	ε	7	20.7 (0.3)	70.7 (0.9)	8.6 (1.0)	100.0	2	0.22 (0.00)	0.76 (0.01)	0.83 (0.10)	0.98	0.226
		α	6	32.7 (0.8)	60.6 (1.2)	6.7 (1.2)	100.0	2	0.35 (0.01)	0.65 (0.01)	0.64 (0.12)	1.00	0.350
OD1292-4	0.375	α	6	35.8 (0.7)	57.0 (2.5)	7.2 (0.7)	100.0	2	0.38 (0.01)	0.60 (0.03)	0.67 (0.06)	0.98	0.386
OD1288-2	0.5	α	4	48.0 (0.3)	46.3 (0.7)	5.7 (0.5)	100.0	2	0.50 (0.00)	0.48 (0.01)	0.53 (0.05)	0.99	0.509
OD1292-5	0.75	α	7	73.4 (0.7)	23.6 (0.4)	3.0 (0.6)	100.0	2	0.75 (0.01)	0.24 (0.00)	0.27 (0.05)	0.99	0.757
T = 1100ºC													
OD1347-6	0	ε	6	0.2 (0.2)	88.1 (0.7)	11.7 (0.9)	100.0	2	0.00 (0.00)	0.96 (0.01)	1.12 (0.08)	0.96	0.003
		Hem	6	0.1 (0.1)	101.8 (2.0)		101.9	3	0.00 (0.00)	2.00 (0.04)		2.00	0.001
OD1347-1	0.125	ε	6	12.7 (0.7)	76.4 (1.1)	11.0 (1.0)	100.0	2	0.13 (0.01)	0.81 (0.01)	1.03 (0.09)	0.95	0.143
		Hem*	7	4.6 (1.6)	95.4 (2.4)		100.0	3	0.09 (0.03)	1.88 (0.05)		1.97	0.046
OD1347-3	0.25	ε	6	20.1 (0.9)	71.8 (1.1)	8.1 (1.2)	100.0	2	0.22 (0.01)	0.78 (0.01)	0.78 (0.12)	1.00	0.218
		α	9	28.5 (1.1)	64.4 (1.7)	7.1 (1.1)	100.0	2	0.31 (0.01)	0.70 (0.02)	0.68 (0.11)	1.00	0.307
		Hem*	6	4.5 (0.9)	99.0 (1.0)		103.6	3	0.09 (0.02)	1.89 (0.02)		1.97	0.044
OD1347-4	0.375	α	6	36.1 (0.7)	57.8 (0.9)	6.2 (0.7)	100.0	2	0.39 (0.01)	0.62 (0.01)	0.59 (0.07)	1.01	0.384
T = 1200ºC													
OD1291-1	0.125	α	4	24.6 (1.2)	68.0 (1.3)	7.4 (1.9)	100.0	2	0.27 (0.01)	0.74 (0.01)	0.71 (0.19)	1.01	0.266
		Hem	3	4.7 (0.3)	97.5 (0.4)		102.2	3	0.09 (0.01)	1.88 (0.01)		1.97	0.046
OD1291-3	0.25	α	6	30.5 (0.6)	63.2 (1.3)	6.3 (1.4)	100.0	2	0.33 (0.01)	0.69 (0.01)	0.61 (0.13)	1.02	0.326
		Hem	3	5.6 (0.2)	97.0 (1.7)		102.6	3	0.11 (0.00)	1.86 (0.03)		1.96	0.055
OD1291-4	0.375	α	6	39.6 (0.7)	53.9 (1.1)	6.5 (1.7)	100.0	2	0.42 (0.01)	0.57 (0.01)	0.61 (0.16)	0.99	0.424
		Hem	6	7.2 (0.2)	96.0 (0.7)		103.2	3	0.14 (0.00)	1.82 (0.01)		1.95	0.070
OD1291-2	0.5	α	6	49.2 (0.8)	45.1 (0.8)	5.7 (1.1)	100.0	2	0.51 (0.01)	0.47 (0.01)	0.53 (0.10)	0.99	0.522
		Hem	5	9.5 (2.3)	91.7 (1.5)		101.2	3	0.18 (0.04)	1.76 (0.03)		1.94	0.094
T = 1300ºC													
OD1298-3	0.25	α	6	35.2 (0.5)	57.7 (0.9)	7.1 (1.4)	100.0	2	0.37 (0.01)	0.61 (0.01)	0.67 (0.13)	0.99	0.379
		Hem	6	7.0 (0.2)	95.9 (1.0)		102.8	3	0.13 (0.00)	1.82 (0.02)		1.96	0.068
OD1298-2	0.5	α	6	49.3 (0.3)	45.5 (0.5)	5.3 (0.5)	100.0	2	0.52 (0.00)	0.48 (0.01)	0.49 (0.05)	1.00	0.520
		Hem	6	9.7 (1.0)	93.3 (2.1)		103.0	3	0.18 (0.02)	1.76 (0.04)		1.94	0.094
OD1298-5	0.75	α	6	73.4 (0.8)	23.2 (0.7)	3.4 (1.2)	100.0	2	0.75 (0.01)	0.24 (0.01)	0.31 (0.11)	0.98	0.760
T = 1400ºC													
OD1334-1	0.125	α_H*	4	32.5 (0.0)	61.2 (1.0)	6.3 (1.0)	100.0	2	0.35 (0.00)	0.66 (0.01)	0.61 (0.09)	1.01	0.347
		α_L	6	23.3 (0.4)	70.5 (1.3)	6.2 (1.4)	100.0	2	0.26 (0.00)	0.78 (0.01)	0.61 (0.14)	1.04	0.248
		Hem	8	7.3 (0.3)	96.5 (1.0)		103.8	3	0.14 (0.00)	1.82 (0.02)		1.95	0.070
OD1334-3	0.25	α	6	34.5 (0.5)	57.5 (0.9)	8.0 (1.2)	100.0	2	0.36 (0.00)	0.60 (0.01)	0.74 (0.11)	0.97	0.375
		Hem	6	8.0 (0.4)	94.7 (0.8)		102.7	3	0.15 (0.01)	1.80 (0.02)		1.95	0.078
OD1334-2	0.5	α	6	49.5 (1.0)	45.5 (1.0)	5.0 (1.5)	100.0	2	0.52 (0.01)	0.48 (0.01)	0.47 (0.14)	1.00	0.521
		Hem	6	10.8 (0.2)	92.8 (0.7)		103.7	3	0.20 (0.00)	1.73 (0.01)		1.93	0.104
OD1334-5	0.75	α	6	73.2 (0.5)	23.4 (0.6)	3.5 (0.7)	100.0	2	0.74 (0.01)	0.24 (0.01)	0.31 (0.07)	0.98	0.758

T = 1500ºC														
OD1336-1	0.125	α*	9	20.7 (0.6)	71.3 (1.2)	8.0 (1.6)	100.0	2	0.23 (0.01)	0.78 (0.01)	0.77 (0.16)	1.00	0.225
		Hem	6	7.9 (0.1)	95.2 (1.2)		103.1	3	0.15 (0.00)	1.80 (0.02)		1.95	0.077
OD1336-2	0.5	α_H	6	49.4 (1.1)	44.1 (0.5)	6.5 (1.0)	100.0	2	0.51 (0.01)	0.46 (0.00)	0.59 (0.09)	0.97	0.528
		α_L	3	44.5 (0.4)	50.6 (1.2)	4.9 (1.3)	100.0	2	0.48 (0.00)	0.54 (0.01)	0.47 (0.12)	1.02	0.468
		Hem	3	12.1 (0.4)	90.2 (1.5)		102.3	3	0.23 (0.01)	1.70 (0.03)		1.92	0.119
OD1336-5	0.75	α	6	73.5 (1.3)	23.6 (0.5)	2.9 (1.5)	100.0	2	0.75 (0.01)	0.24 (0.00)	0.26 (0.14)	0.99	0.757
OD1336-7	1	α	6	100.7 (1.1)	0.0 (0.1)		100.8	2	1.00 (0.01)	0.00 (0.00)		1.00	1.000
T = 1600ºC														
OD1338-1	0.125	Hem	7	8.5 (0.3)	92.4 (2.4)		100.9	3	0.16 (0.01)	1.78 (0.05)		1.95	0.084
		Melt	2	12.6 (1.0)	62.7 (3.8)		75.3	2	0.21 (0.02)	1.05 (0.06)		1.26	0.168
OD1338-4	0.375	α_H*	6	49.2 (0.9)	47.7 (0.7)	3.0 (1.0)	100.0	2	0.54 (0.01)	0.52 (0.01)	0.29 (0.09)	1.06	0.508
		α_L*	6	35.7 (0.6)	61.6 (1.0)	2.7 (1.2)	100.0	2	0.41 (0.01)	0.70 (0.01)	0.27 (0.12)	1.11	0.367
		Melt	4	27.4 (0.7)	56.6 (0.9)		84.0	2	0.39 (0.01)	0.81 (0.01)		1.20	0.326
OD1338-2	0.5	α_H	5	58.9 (1.0)	36.7 (0.4)	4.3 (1.2)	100.0	2	0.61 (0.01)	0.38 (0.00)	0.40 (0.12)	1.00	0.616
		α_L	6	48.5 (1.1)	45.9 (1.4)	5.6 (1.5)	100.0	2	0.51 (0.01)	0.48 (0.01)	0.52 (0.14)	0.99	0.514
		Melt	3	27.2 (0.6)	55.1 (1.1)		82.4	2	0.40 (0.01)	0.80 (0.02)		1.20	0.331
OD1338-5	0.75	α	6	72.9 (1.3)	23.2 (0.3)	3.8 (1.8)	100.0	2	0.74 (0.01)	0.23 (0.00)	0.35 (0.16)	0.97	0.758

Abbreviations for phases are the same as those in Table 1.

Analyses results for both phases of fine lamellae texture are included.

Numbers in the parentheses arestandard deviation of multiple analyses on the phase.
a Number of analyses.
b H_2O content was calculated from total loss.

Table A1. Chemical composition of FeTi-rich minerals in basalt + H_2O system

		OD1311		OD1168			
	Starting material	10 GPa, 1000°C		12 GPa, 1000°C			
		FeTi		FeTi-1		FeTi-2	
n [a]		3		7		4	
SiO_2	47.22	0.64	(0.15)	2.22	(2.24)	3.25	(2.04)
TiO_2	1.06	90.89	(1.00)	7.98	(0.67)	46.46	(1.11)
Al_2O_3	12.98	0.68	(0.12)	1.87	(0.74)	2.37	(0.35)
Cr_2O_3	-	0.00	(0.01)	0.01	(0.01)	0.04	(0.03)
FeO [b]	11.51	2.52	(0.11)	73.75	(3.33)	32.31	(0.48)
MnO	0.19	0.00	(0.00)	0.06	(0.03)	0.03	(0.01)
MgO	11.93	0.25	(0.03)	2.47	(0.74)	1.72	(0.40)
CaO	8.71	0.47	(0.20)	0.85	(0.82)	0.70	(0.16)
Na_2O	1.81	0.05	(0.02)	0.07	(0.10)	0.09	(0.08)
K_2O	0.37	0.05	(0.02)	0.04	(0.01)	0.02	(0.01)
P_2O_5	0.09	-					
NiO	-	0.02	(0.03)	0.02	(0.02)	0.01	(0.01)
H_2O	3.50	-					
Total	99.36	95.57		89.33		87.00	
Ti/(Fe + Ti) [c]		0.970	(0.001)	0.089	(0.008)	0.564	(0.007)

Notes: Numbers in parentheses denotes standard deviations.

a Number of analyses.

b Iron content is calculated as FeO because analyses were carried out using same standard conditions as coexisting Fe^{2+}-bearing silicate minerals. However, majority of iron in the FeTi-rich minerals is estimated to be Fe^{3+} based on this study.

c Molar ratio.

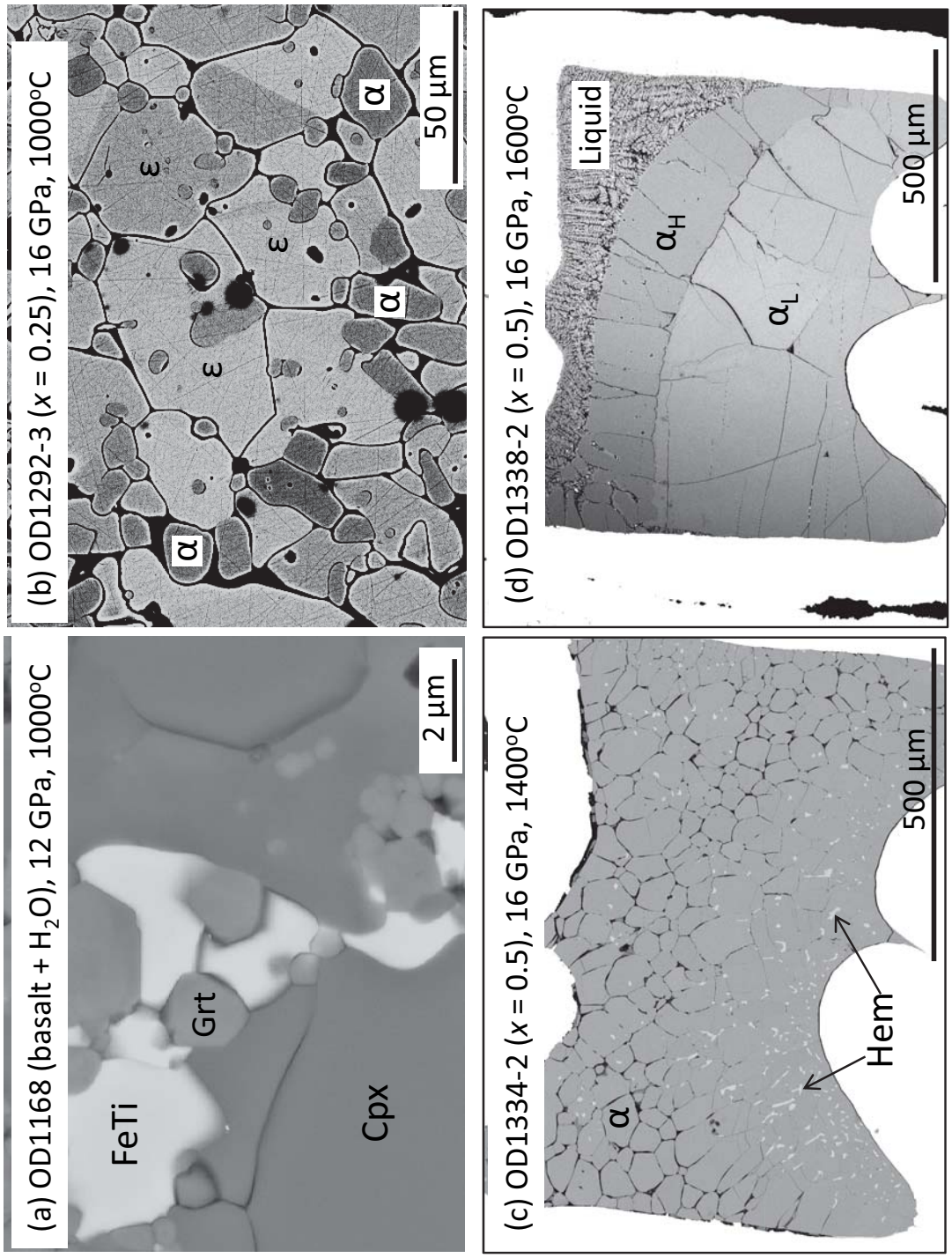
(a) OD1168 (basalt + H_2O), 12 GPa, 1000°C
FeTi
Grt
Cpx
2 µm
(b) OD1292-3 (x = 0.25), 16 GPa, 1000°C
α
ε
ε
ε
α
α
50 µm
(c) OD1334-2 (x = 0.5), 16 GPa, 1400°C
α
Hem
500 µm
(d) OD1338-2 (x = 0.5), 16 GPa, 1600°C
Liquid
α_H
α_L
500 µm

Figure 1

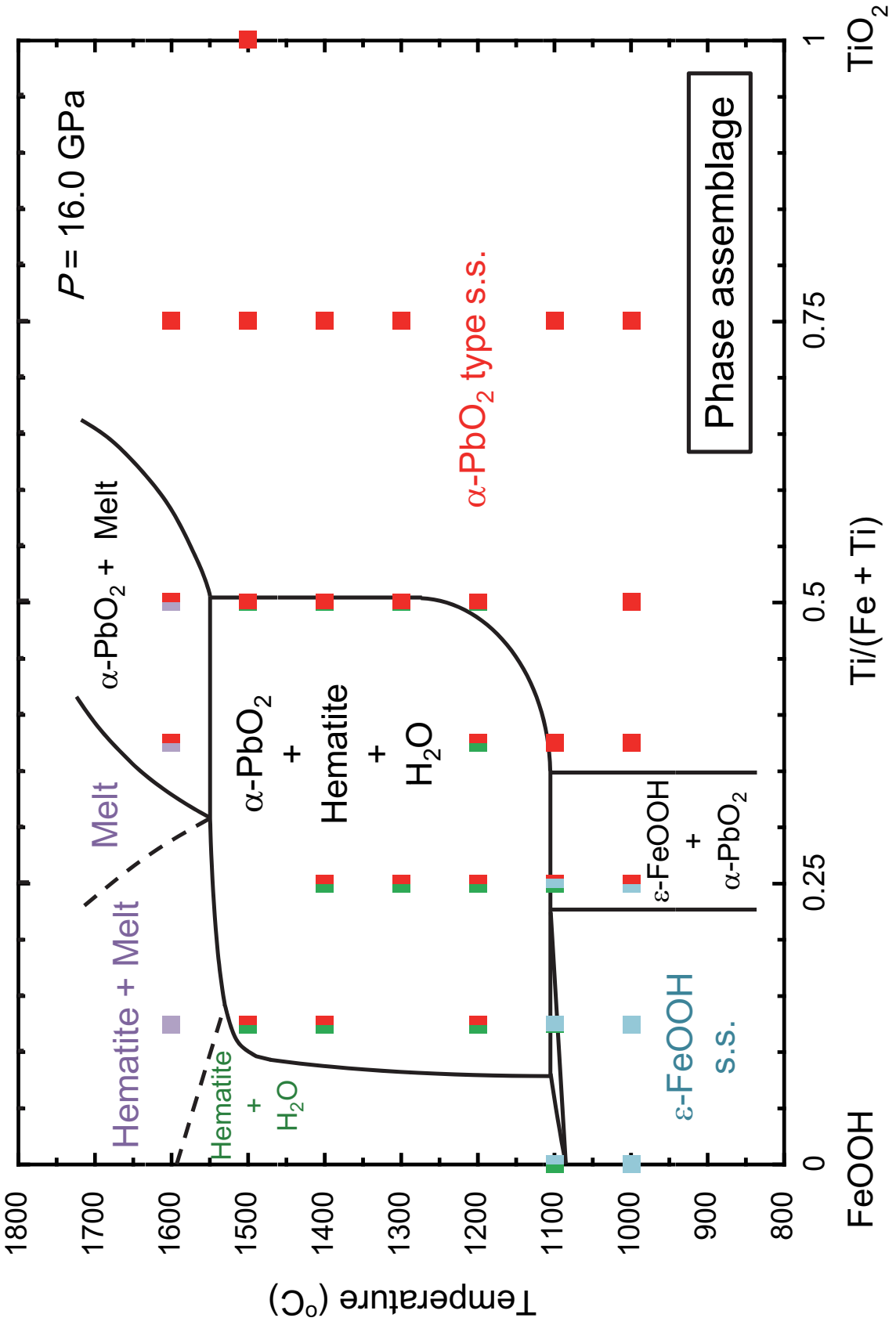
P = 16.0 GPa
Phase assemblage
α-PbO2 type s.s.
α-PbO2 + Melt
Melt
Hematite + Melt
α-PbO2 + Hematite + H2O
Hematite + H2O
ε-FeOOH + α-PbO2
ε-FeOOH s.s.
Temperature (°C)
1800
1700
1600
1500
1400
1300
1200
1100
1000
900
800
FeOOH
0
0.25
0.5
0.75
1
TiO2
Ti/(Fe + Ti)

Figure 2

This is a preprint, the final version is subject to change, of the American Mineralogist (MSA)
Cite as Authors (Year) Title. American Mineralogist, in press.
(DOI will not work until issue is live.) DOI: http://dx.doi.org/10.2138/am-2016-5517

Figure 3

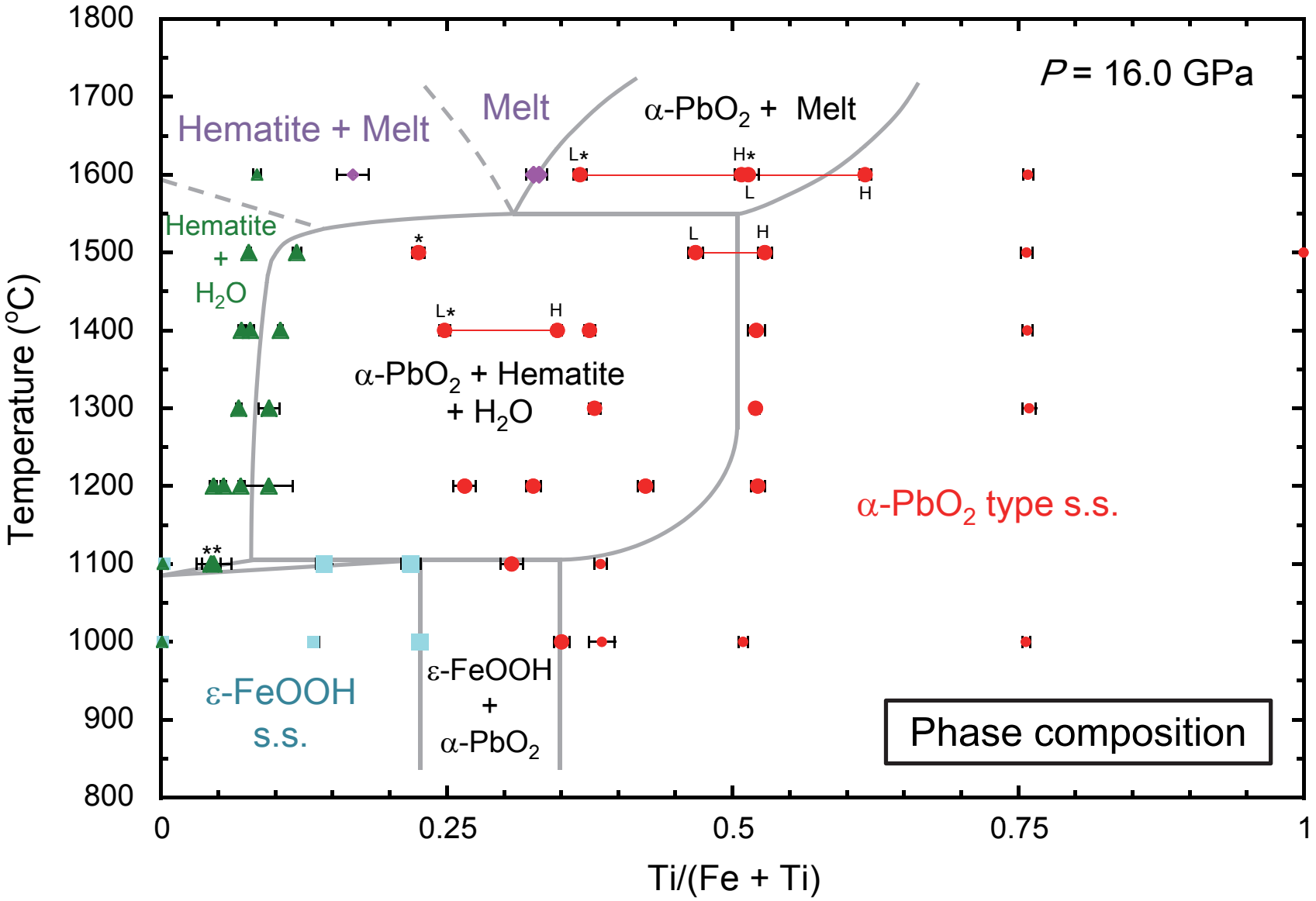

This is a preprint, the final version is subject to change, of the American Mineralogist (MSA)
Cite as Authors (Year) Title. American Mineralogist, in press.
(DOI will not work until issue is live.) DOI: http://dx.doi.org/10.2138/am-2016-5517

Figure 4

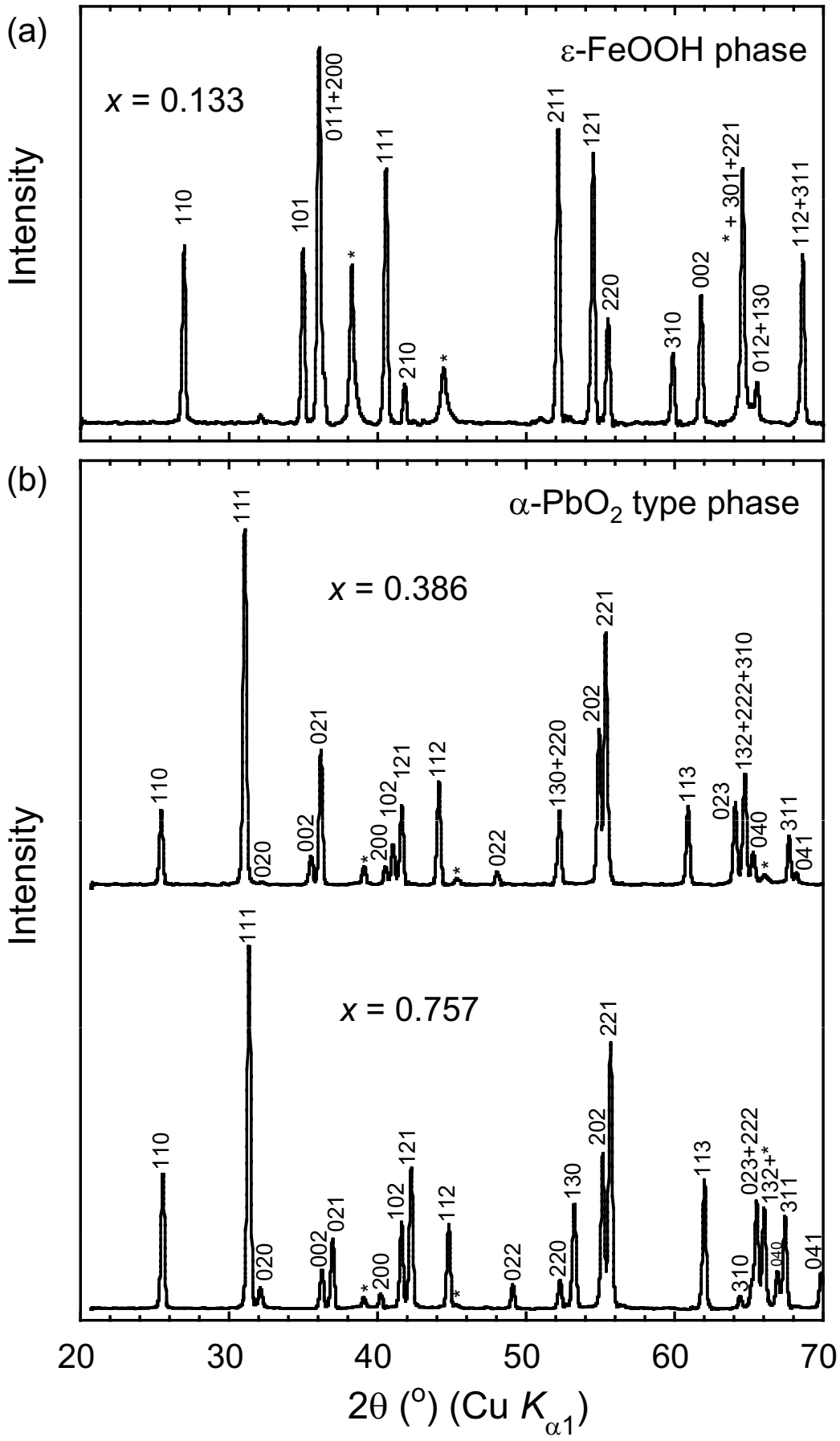

This is a preprint, the final version is subject to change, of the American Mineralogist (MSA)
Cite as Authors (Year) Title. American Mineralogist, in press.
(DOI will not work until issue is live.) DOI: http://dx.doi.org/10.2138/am-2016-5517

Figure 5

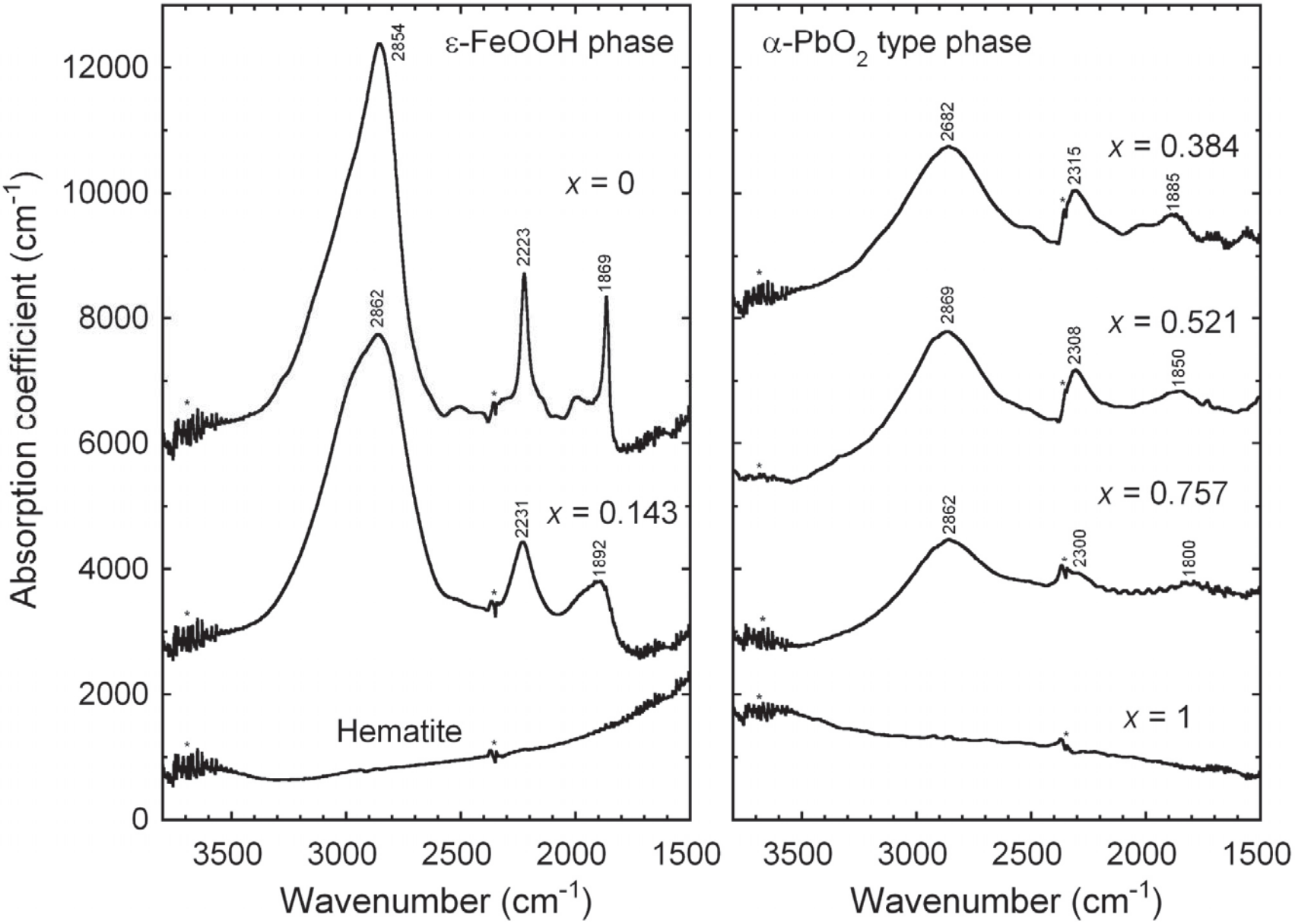

Figure 6

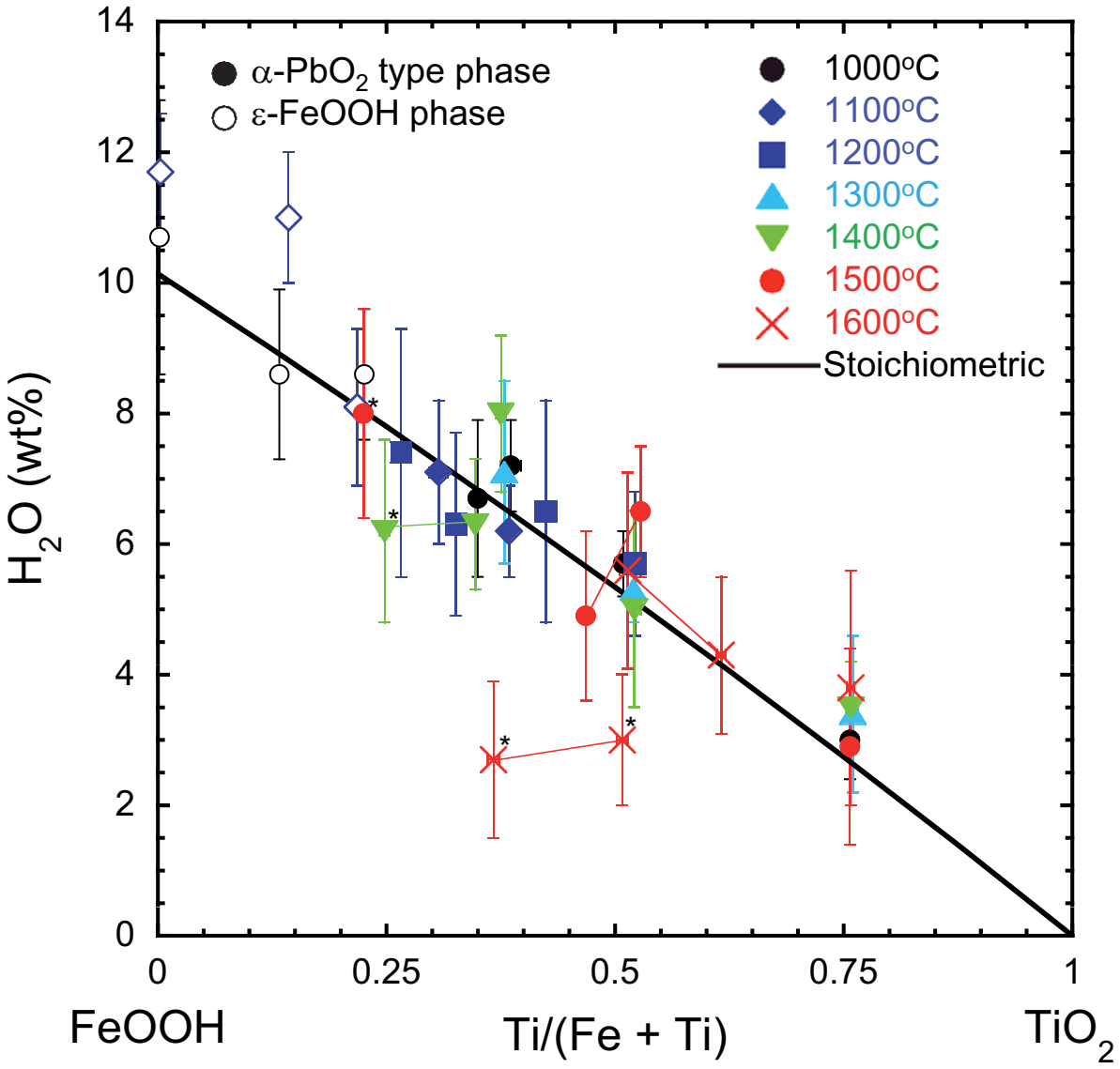
α-PbO2 type phase
ε-FeOOH phase
1000°C
1100°C
1200°C
1300°C
1400°C
1500°C
1600°C
Stoichiometric
H2O (wt%)
0
2
4
6
8
10
12
14
0
0.25
0.5
0.75
1
FeOOH
Ti/(Fe + Ti)
TiO2

Figure 7

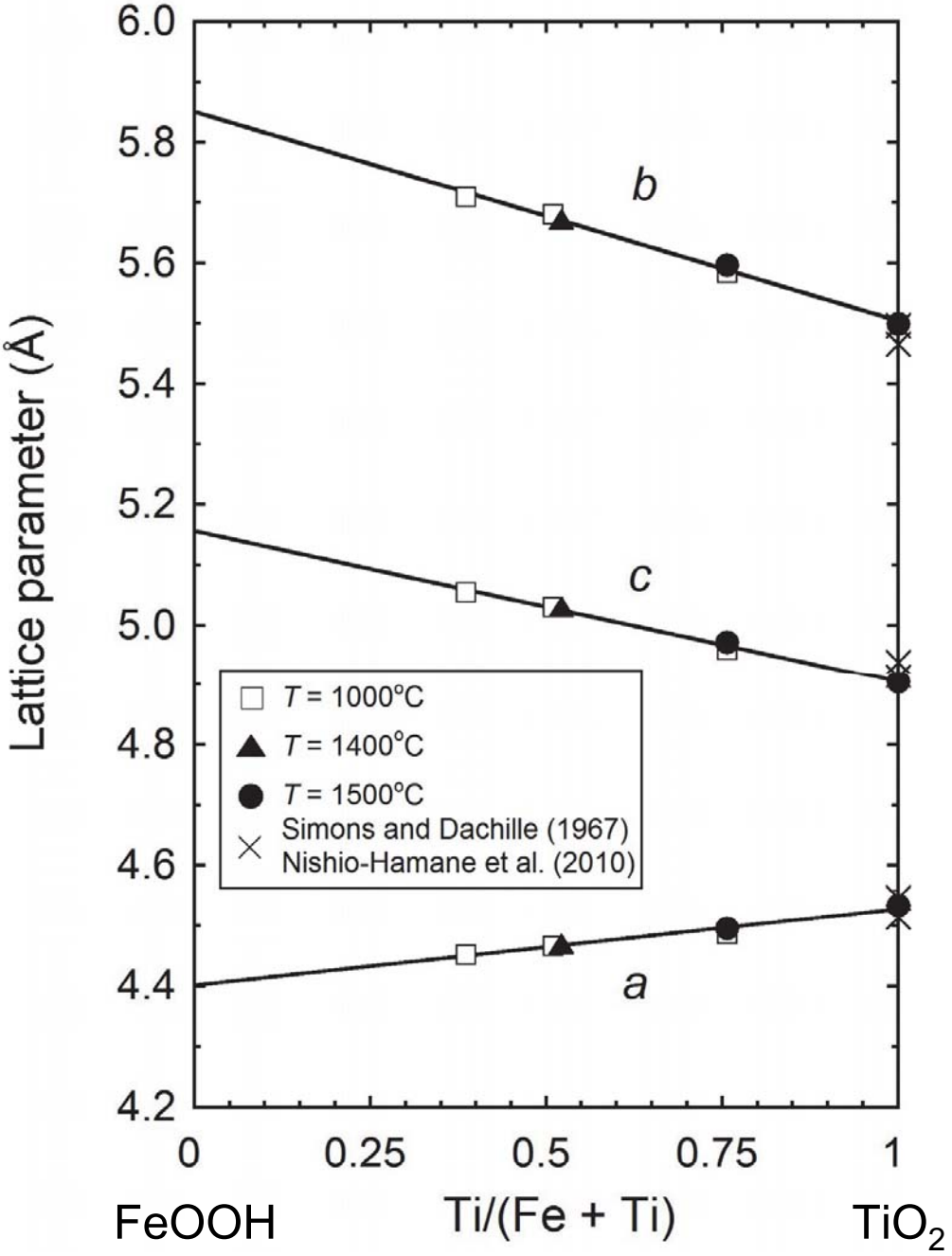
6.0
5.8
5.6
5.4
5.2
5.0
4.8
4.6
4.4
4.2
Lattice parameter (Å)
b
c
a
T = 1000°C
T = 1400°C
T = 1500°C
Simons and Dachille (1967)
Nishio-Hamane et al. (2010)
0
0.25
0.5
0.75
1
FeOOH
Ti/(Fe + Ti)
TiO2

This is a preprint, the final version is subject to change, of the American Mineralogist (MSA)
Cite as Authors (Year) Title. American Mineralogist, in press.
(DOI will not work until issue is live.) DOI: http://dx.doi.org/10.2138/am-2016-5517

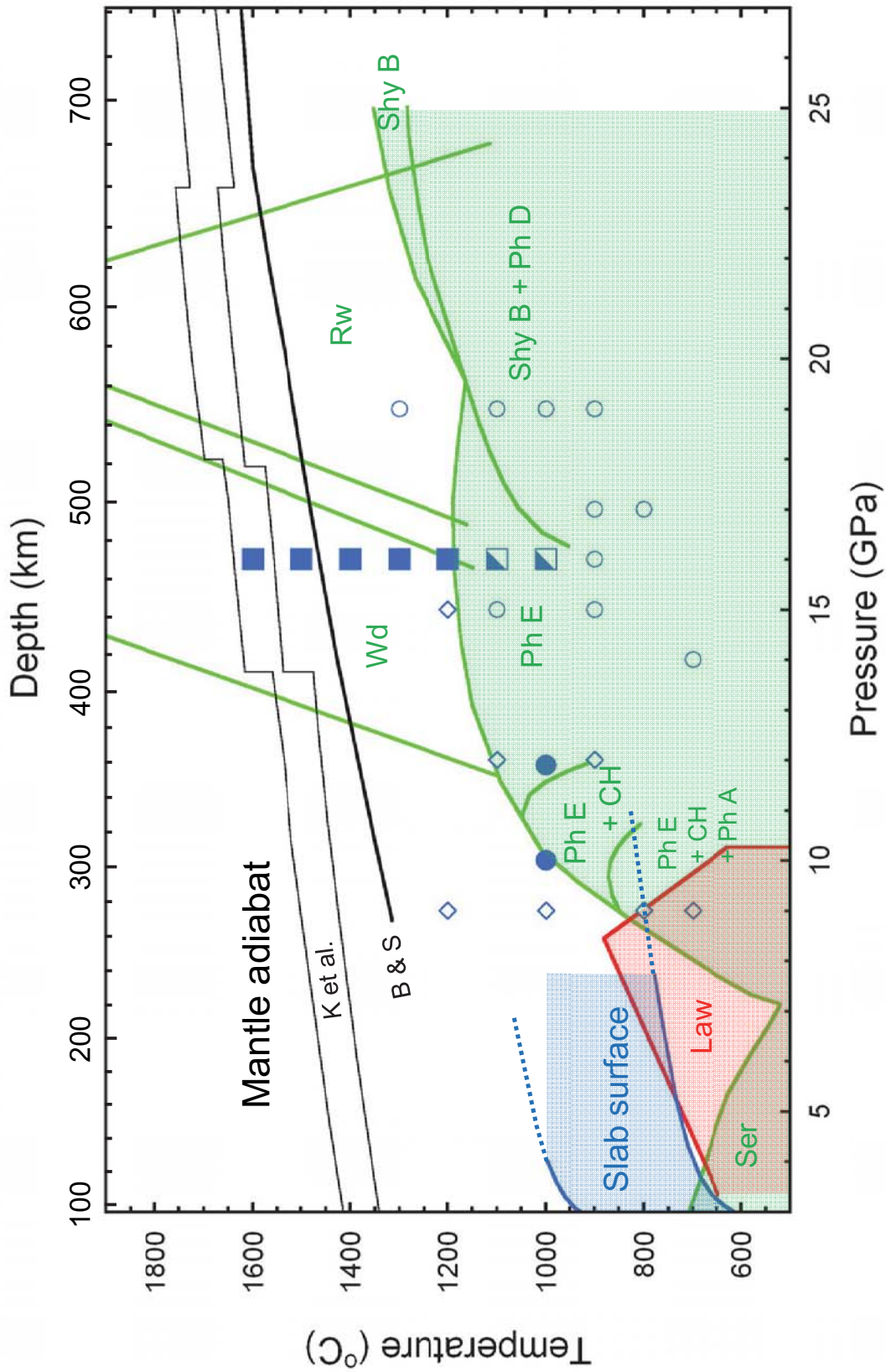

Figure 8